EMERGENT SYMBOL-LIKE NUMBER VARIABLES IN ARTIFICIAL NEURAL NETWORKS

Anonymous authors
Paper under double-blind review

ABSTRACT

There is an open question of what types of numeric representations can emerge in neural systems. To what degree do neural networks induce abstract, mutable, slot-like numeric variables, and in what situations do these representations emerge? How do these representations change over the course of learning, and how can we understand the neural implementations in ways that are unified across different models' implementations? In this work, we approach these questions by first training sequence based neural systems using Next Token Prediction (NTP) objectives on numeric cognitive tasks. We then seek to understand the neural solutions at the level of causal abstractions or symbolic programs. We use a combination of causal interventions and visualization methods to find that models of sufficient dimensionality do indeed develop strong analogs of interchangeable, mutable number variables purely from the NTP objective. We then ask how variations on the tasks and model architectures affect the models' learned solutions to find that these symbol-like numeric representations do not form for every variant of the task, and transformers solve the problem differently than their recurrent counterparts. Lastly, we show that in all cases, some degree of gradience exists in the neural symbols, highlighting the difficulty of finding simple, interpretable symbolic stories of how neural networks perform numeric tasks. Taken together, our results are consistent with the view that neural networks can approximate interpretable symbolic programs of number cognition, but the particular program they approximate and the extent to which they approximate it can vary widely, depending on the network architecture, training data, extent of training, and network size.

1 INTRODUCTION

Both biological and artificial Neural Networks (NNs) have powerful modeling abilities. We can see an example of this in biological NNs (BNNs) from the impressive capabilities of human cognition, and we can see this in artificial NNs (ANNs) where recent advances have had such great success that ANNs have been crowned the "gold standard" in many machine learning communities (Alzubaidi et al., 2021). The inner workings of NNs, however, are still often opaque. This is, in part, due to their representations being highly distributed. Individual neurons can play multiple roles within a network (Rumelhart et al., 1986; McClelland et al., 1986; Smolensky, 1988; Olah et al., 2017; 2020; Elhage et al., 2022; Scherlis et al., 2023; Olah, 2023).

Symbolic algorithms/programs, in contrast, defined as processes that manipulate distinct, typed entities according to explicit rules and relations, can have the benefit of consistency, transparency, and generalization when compared to their neural counterparts. A concrete example of a symbolic algorithm is a computer program, where the variables are abstract, mutable entities, able to represent many different values, and these variables are processed by well defined functions. Human designed symbolic systems, however, can lack the expressivity and performance of NNs. This is apparent in the field of natural language processing where neural architectures trained on vast amounts of data (Vaswani et al., 2017; Brown et al., 2020; Kaplan et al., 2020) have swept the field, surpassing the pre-existing symbolic approaches. Furthermore, there are many existing theories that posit the necessity of algorithmic, symbolic, processing for higher level cognition (Do & Hasselmo, 2021; Fodor & Pylyshyn, 1988; Fodor, 1975; 1987; Newell, 1980; 1982; Pylyshyn, 1980; Marcus, 2018; Lake et al., 2017). While the aforementioned successes of neural systems may call such cognitive claims into question, it might be argued that neural systems actually implement such symbolic algorithms; or,

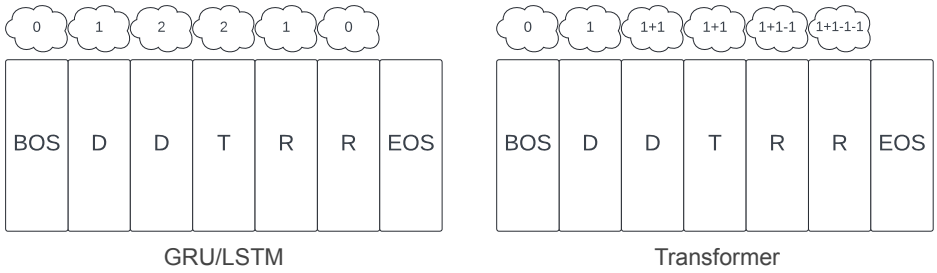

Figure 1: Visual depiction of different architecture's solutions achieving the same accuracy on the same numeric equivalence task. The rectangles represent token types for a task in which the T token indicates that the model must produce the same number of Rs as it witnessed Ds, and must end the sequence with an EOS (see Methods for more details). The thought bubbles represent causally discovered, neural variables encoded within subspaces of the models' representations. The recurrent models encode a mutable count that increments up and then back down to indicate the end of the task. Transformers learn a solution in which they recompute the task relevant information from the context in their attention at each step in the sequence. All NoPE transformers align with the displayed solution, where they assign opposite numeric values to the D and R tokens and then recompute their sum in the attention mechanism at each step in the sequence, knowing to stop when the difference equals 0. RoPE transformers trained on a variant of the task that breaks number-positional correlations also align to this specific solution.

they may approximate them well enough that seeking to find the most aligned symbolic algorithm would be a powerful step toward an accessible, unified understanding of the complex neural behavior. This approach of seeking to characterize the mechanisms of a NN-based system in terms of the most aligned symbolic algorithm is, in some sense, the goal of most cognitive science, neuroscience, and mechanistic interpretability.

In this work, we narrow our focus to numeric cognition and ask, how we can understand neural implementations of numeric concepts at the level of symbolic algorithms? Numeric reasoning has the advantage of being well studied in humans of different ages and with different numeric experience, providing a powerful domain for comparisons between BNNs and ANNs (Di Nuovo & Jay, 2019). We focus on a numeric equivalence task that was used to test the numeric abilities of humans whose language lacks explicit number words (Gordon, 2004). The task is formulated as a sequence of tokens, requiring the subject to produce the same number of response tokens as a quantity of demonstration tokens initially observed at the beginning of the task. This task is interesting for computational settings because the training labels vary in both type and length, and the numeric structures of interest are never explicitly labeled. Similar versions of this task have also used in previous theoretical and computational work (El-Naggar et al., 2023; Weiss et al., 2018; Behrens et al., 2024). These works provide a platform to expand upon in order to understand how to unify seemingly disparate systems.

What sorts of representations do ANNs use to solve such a task and how do they arrive at these representations? Do the networks represent numbers in a unified number system? Do they use different solutions for different situations? Do the answers to these questions change over the course of training, and do the answers vary based on task and architectural details? How can we unify these solutions in satisfying ways for cognitive scientists, neuroscientists, and computer scientists alike? We wish to understand the degree to which a neural system might implement a mutable, abstract numeric variable, similar to the kind we might assign to an allocated storage location in a computer program.

In this work, we pursue these interests by training recurrent and attention based ANNs on Next Token Prediction (NTP) tasks and perform both causal and correlative analyses to understand their neural solutions. Our contributions are as follows:

1. We find causal alignments between neural variables (subspaces of the activations) and symbolic/causal variables from a counting program that increments and decrements a count variable.

2. We show that transformer architectures solve the task by referencing and recomputing information from the context at each step in the sequence, contrasted against the recurrent solution of storing a cumulative, Markovian state.
3. We show the importance of finding aligned neural subspaces for causal interventions, rather than causally intervening directly on activations.
4. We show that the recurrent models' alignment to the counting program can be strongly influenced by task details that are seemingly unrelated to the underlying numeric principles.
5. We show that the symbol-like neural variables are graded, with inferior interchangeability between larger numbers and between numbers that have a greater difference in magnitude.
6. We examine the neural variables over the course of training to find a correlation between task accuracy and strength of the alignment.
7. Lastly, we show an effect of model size, where models of minimal size have a greater degree of gradience in their alignment, while larger models have more precise neural variables.

We use these results to encourage use of multiple interpretability tools for any representational analysis, to highlight functional differences that might emerge from architectural constraints like Markovian states vs attention based structures, and to highlight the varying degrees of gradience in neural implementations of causal variables—adding to discussions on mechanistic interpretability.

2 Related Work

We wish to highlight the importance of using causal manipulations for interpreting neural functions in this work. Causal inference broadly refers to methods that isolate the particular effects of individual components within a larger system (Pearl, 2010). An abundance of causal interpretability variants have been used to determine what functions are being performed by the models' activations (or circuits) (Olah et al., 2018; 2020; Wang et al., 2022; Geva et al., 2023; Merrill et al., 2023; Bhaskar et al., 2024; Wu et al., 2024). Vig et al. (2020) is a recent review that provides an integrative review of the rationale for and utility of causal mediation in neural model analyses. We rely heavily on DAS for our analyses. This method can be thought of as a specific type of activation patching (also referred to as causal tracing) (Meng et al., 2023; Vig et al., 2020). DAS mainly differs from the other methods in that it uses a learned rotation matrix to target a specific subspace for the substitutions.

Many publications explore ANNs' abilities to perform counting tasks (Di Nuovo & McClelland, 2019; Fang et al., 2018; Sabathiel et al., 2020; Kondapaneni & Perona, 2020; Nasr et al., 2019; Zhang et al., 2018; Trott et al., 2018). Our tasks and modeling paradigms differ from many of these publications in that numbers are only latent in the structure of our tasks without explicit teaching of distinct symbols for distinct numeric values. El-Naggar et al. (2023) provided a theoretical treatment of Recurrent Neural Network (RNN) solutions to a parentheses closing task, and Weiss et al. (2018) explored Long Short-Term Memory RNNs (LSTMs) (Hochreiter & Schmidhuber, 1997) and Gated Recurrent Units (GRUs) (Cho et al., 2014) in a similar numeric equivalence task looking at the activations. These works showed correlates of a magnitude scaling solution in both theoretical and practically trained ANNs. Our work builds on their findings by using causal methods for our analyses, and by expanding the models considered. Lastly, we mention Behrens et al. (2024), who explored transformer counting solutions in a task similar to ours. Our work builds upon their findings by including positional encodings in our transformers and providing causal interventions.

3 Methods

In this work, we train models on numeric equivalence tasks and then use interpretability methods such as Distributed Alignment Search (DAS) (Geiger et al., 2021; 2023) to understand the manner in which the models solve the task.

3.1 Numeric Equivalence Tasks

Each task we consider is defined by varying length sequences of tokens. Each sequence starts with a Beginning of Sequence (BOS) token and ends with an End of Sequence (EOS) token. Each sequence

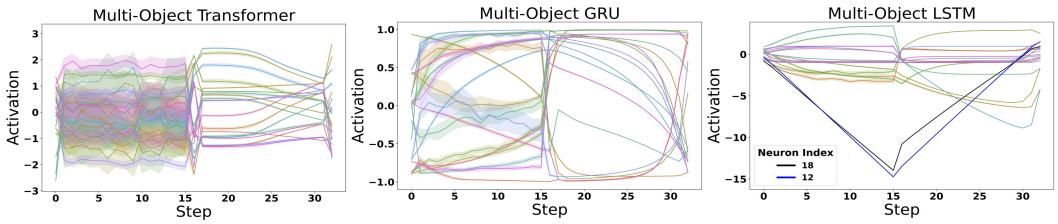

Figure 2: The activation values for each neuron at each step in the trial with a target count of 15 for individual models. Values are averaged over 15 trials. We highlight the specific neurons used in a causal intervention described in Sections 3.5 and 4.1.

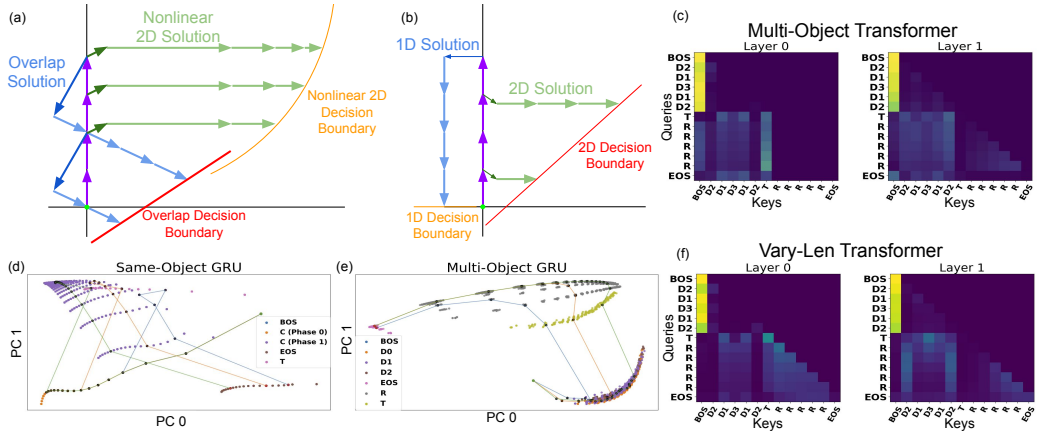

Figure 3: (a) and (b) Theoretical neural solutions to the numeric tasks. The purple arrows represent incoming demo tokens, the darker arrows indicate the trigger token, the lighter colored arrows indicate increments to the response tokens, the green dot indicates the starting point. (d) and (e) show the first two principal components of a Same-Object and Multi-Object GRUs. Multiple trajectories are shown, each point is a projected latent state in a trajectory. The lines trace individual trajectories. (See Appendix 17 and 15 for expanded details.) (c) and (f) show the attention weights for different transformers in the Multi-Object Task (see Supplement A.6 for details).

is defined by a uniformly sampled target quantity from the inclusive range of 1 to 20. The sequence is constructed as the combination of two phases. The first phase, called the demonstration phase (**demo phase**), starts with the BOS token and continues with a series of demo tokens equal in quantity to the sampled target quantity. Following the demo tokens is the Trigger token (T), indicating the end of the demo phase and the beginning of the response phase (**resp phase**). The resp phase consists of a series of resp tokens equal in number to target quantity. The EOS token follows the resp tokens, denoting the end of the sequence.

During the initial model training, we include all tokens in the autoregressive loss. During model evaluation and DAS trainings, we only consider tokens in the resp phase—which are fully determined by the demo phase. During model trainings, we hold out the target quantities 4, 9, 14, and 17. A trial is considered correct when all resp tokens and the EOS token are correctly predicted by the model after the trigger. We include three variants of this task differing only in their demo and resp token types.

Multi-Object Task: there are 3 demo token types $\{D_1, D_2, D_3\}$ with a single response token type, R. The demo tokens are uniformly sampled from the 3 possible token types. An example sequence with a target quantity of 2 could be: "BOS D_3 D_1 T R R EOS"

Single-Object Task: there is a single demo token type, D, and a single response token type, R. An example with a target quantity of 2 is: "BOS D D T R R EOS"

Same-Object Task: there is a single token type, C, used by both the demo and resp phases. An example with a target quantity of 2 would be: "BOS C C T C C EOS".

3.2 Model Architectures

The recurrent models in this paper consist of Gated Recurrent Units (GRUs) (Cho et al., 2014), and Long Short-Term Memory networks (LSTMs) (Hochreiter & Schmidhuber, 1997). These architectures both have a Markovian, hidden state vector that bottlenecks all predictive computations following the structure:

$$h_{t+1} = f(h_t, x_t) \tag{1}$$

$$\hat{x}_{t+1} = g(h_{t+1}) \tag{2}$$

Where h_t is the hidden state vector at step t, x_t is the input token at step t, f is the recurrent function (either a GRU or LSTM cell), and g is a multi-layer perceptron (MLP) used to make a prediction, denoted $\hat{x}_{t+1}$, of the token at step $t+1$. We contrast the recurrent architectures against transformer architectures (Vaswani et al., 2017; Touvron et al., 2023; Su et al., 2023) in that the transformers use a history of input tokens, $X_t = [x_1, x_2, ..., x_t]$, at each time step, t, to make a prediction:

$$\hat{x}_{t+1} = f(X_t) \tag{3}$$

Where f now represents the transformer architecture. We show results from 2 layer, single attention head transformers that use RoPE positional encodings (Su et al., 2023). Refer to Supplement A.4 and Figure 7 for more model and architectural details. We consider transformers with No Positional Encodings (NoPE) in Supplemental section A.4. Except for in the training curves in Figure 5, we first train the models to >99.99% accuracy on their respective tasks before performing analyses. The models are evaluated on 15 sampled sequences of each of the 16 trained and 4 held out target quantities. We train 6 model seeds for each training condition. Model seeds that failed to achieve this standard were dropped from the analyses, including 3 model seeds from the LSTM models in the Same-Object task and one seed from the transformer models in each of the Single-Object and Same-Object tasks.

3.3 Symbolic Programs

In this work, we examine the alignment of 3 different symbolic programs to the models' distributed representations.

1. **Up-Down Program:** uses a single numeric variable, called the **Count**, to track the difference between the number of demo tokens and resp tokens at each step in the sequence. It also contains a **Phase** variable to determine whether it is in the demo or resp phase. The program ends when the Count is equal to 0 during the resp phase.
2. **Up-Up Program:** uses two numeric variables—the **Demo Count** and **Resp Count**—in addition to a Phase variable to track quantity at each step in the sequence. This program increments the Demo Count during the demo phase and increments the Resp Count during the resp phase. It ends when the Demo Count is equal to the Resp Count during the resp phase.
3. **Context Distributed (Ctx-Distr) Program:** queries a history of inputs at each step in the sequence to determine when to stop rather than encoding a cumulative quantity variable. A more specific version of this program (that appears to emerge under some conditions) is is one in which the program assigns a value of 1 to each demo token and a -1 to each resp token (or *visa-versa*) and computes their combined sum at each step in the sequence to determine the count. This program knows to stop when the sum is 0.

We include Algorithms 1, 2, and 3 in the supplement which show the pseudocode used to implement the Up-Down, Up-Up, and Ctx-Distr programs in simulations. Refer to Figure 1 for an illustration of the Up-Down strategy and the more specific version of the Ctx-Distr strategy that is only observed in some transformers.

It is important to note that there are an infinite number of causally equivalent implementations of these programs. For example, the Up-Down program could immediately add and subtract 1 from the Count at every step of the task in addition to carrying out the rest of the program as previously described. We do not discriminate between programs that are causally indistinct from one another in this work.

3.4 DISTRIBUTED ALIGNMENT SEARCH (DAS)

DAS is a hypothesis testing framework for finding alignments between distributed systems and symbolic programs/algorithms (also referred to as causal abstractions) by performing interchange interventions (equivalently referred to as causal interventions, patches, or substitutions) (Geiger et al., 2021; 2023). For all DAS experiments, we freeze the model weights before performing the analysis.

In general, DAS measures the degree of alignment between the best subspace of a distributed model's representations with the variables from a specified symbolic program. The method uses causal interventions to both train the alignment and to make claims about the degree of alignment. For a given variable from the symbolic program, DAS learns an orthogonal rotation matrix, $\mathcal{R} \in R^{m \times m}$, that orients a subspace of the distributed representations along a subset of the dimensions in the representation, allowing the subspace to be freely interchanged between representations. The method relies on the notion of counterfactual behavior to train the rotation matrix. For a given symbolic program, we know what the program's behavior should be after performing a causal intervention. This counterfactual behavior can be used as the training signal for the rotation matrices. The matrices are trained to convergence and are then validated on unseen causal interventions to determine the success of the alignment.

Concretely, we uniformly sample a time point from two separate sequences respectively. These time points are t for what we will call the target sequence and u for the source sequence, where *target* refers to the sequence and representations that will be intervened upon, and *source* refers to the sequence and representations that will be harvested from for the intervention. We run the model on each sequence until time point t and u respectively. We then take the latent representations from a prespecified layer in the model at these points t and u. We refer to these representations as the target and source vectors, $h_t^{trg} \in R^m$ and $h_u^{src} \in R^m$, where m is the number of neurons in each distributed representation. We then rotate h_t^{trg} and h_u^{src} using $\mathcal{R}$ resulting in r_t^{trg} and r_u^{src}, and then we replace a pre-specified number of dimensions in r_t^{trg} with the same dimensions from r_u^{src}. Lastly we apply the inverse of the rotation to r_u^{trg} resulting in a new vector, denoted h_t^v. This can be written formally as:

$$h_t^v = \mathcal{R}^{-1}((1 - D)\mathcal{R}h_t^{trg} + D\mathcal{R}h_u^{src}) \tag{4}$$

Where $D \in R^{m \times m}$ is a diagonal, binary matrix used to isolate the desired set of dimensions to replace. In this work, we pre-specify the number of non-zero entries in D to be half of m. The indices of these non-zero dimensions in D are unimportant as the orthogonal matrix can equivalently learn each basis in any row order. Finally, we discard h_u^{src} and allow the model to continue making token predictions from point t in the target sequence using h_t^v. We use the counterfactual behavior (tokens) of the symbolic program as the training sequence in the autoregressive loss to train the rotation matrix.

Once our rotation matrix has converged, we can evaluate the quality of the alignment using the accuracy of the model's predictions on the counterfactual outputs in held out causal interventions. This accuracy has been referred to as the Interchange Intervention Accuracy (IIA) in previous work (Geiger et al., 2023).

For the LSTM architecture, we perform DAS on a concatenation of the h and c recurrent state vectors. In the GRUs, we operate on the recurrent hidden state. In the transformers, we operate on the hidden state following the first transformer layer (see Figure 7). Unless otherwise stated, we use 10000 intervention samples for training and 1000 samples for validation and testing. We uniformly sample target quantities and intervention time points, t and u, for both the original and source sequences in the training, validation, and testing sets. We orthogonalize the rotation matrix using PyTorch's orthogonal parameterization with default settings. We train the rotation matrix for 1000, with a batch size of 512, selecting the checkpoint with the best validation performance for analysis. We use a learning rate of 0.003 and an Adam optimizer.

3.5 ADDITIONAL INTERVENTIONS

A sufficient experiment to demonstrate the lack of use of a cumulative count variable is to look for unchanged behavior after performing a full activation vector substitution on relevant hidden representations. Concretely, one of our tests for the Ctx-Distr is to replace a full activation vector at time step t with the full activation vector at time step u from a different set of inputs. We provide

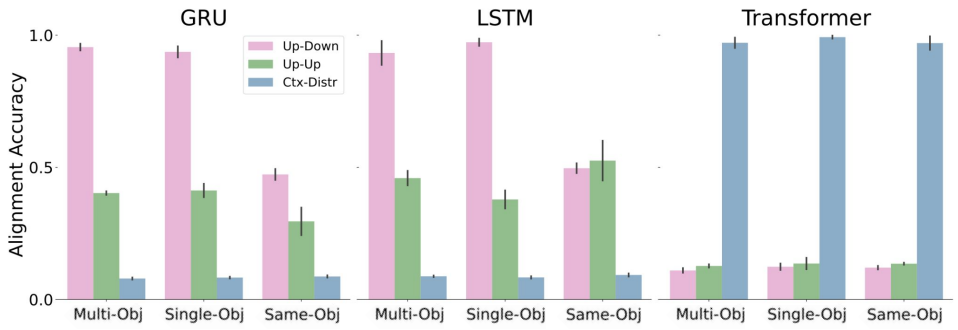

Figure 4: Interchange intervention accuracy (IIA) on variables from different symbolic programs for different tasks faceted by architecture type. The displayed IIA in the Up-Down program is taken from the Count variable. The IIA in the Up-Up program is taken as the better performing of the two possible count variables for each model type respectively. All IIA measurements show the proportion of trials in which the model successfully predicts all counterfactual R and EOS tokens following a causal intervention.

further detail in Supplement A.5 as to why this experiment is sufficient for the claim. We trivially apply these interventions on the recurrent hidden states in the RNNs, and we apply these interventions to the hidden states from Layer 1 in the transformer architectures. If the model is using the Ctx-Distr program, we would expect the models' subsequent token predictions to be unaffected by this intervention. We include a further DAS analysis to align the Last Value variable in the Ctx-Distr program (representing the increment value of the previous input token). These alignments are applied to the embeddings in the GRUs and to the embeddings that are projected into the k and v vectors in the Transformers. We leave the pre-query embeddings unperturbed.

We also include an exploration of direct substitution of individual artificial neuron activation values in the Multi-Object trained models. In these experiments, we directly substitute the activation value of a specific neuron at time step t with the value of the same neuron at time step u from a different sequence. We include one additional activation intervention on the activations of neurons 12 and 18 from the LSTM shown in Figure 2, where we substitute both values in the interventions. In all direct interventions detailed in this section, we evaluate the model's IIA on counterfactual behavior assuming a transfer of the Count.

4 Results

4.1 Causal Abstractions

We first turn our attention to Figure 4 where we can see DAS performance as a function of the causal abstraction used in the alignment. In the recurrent models (GRUs and LSTMs), we see that the most aligned causal abstraction is the Up-Down program. The results are compared against the Up-Up program and the Ctx-Distr program which have significantly lower, albeit non-zero IIAs. We use this as evidence in favor of the interpretation that the recurrent models develop a count up, count down strategy to track quantities within the task.

To determine how the transformer architectures were performing the task, we first looked at the attention weights for both of the two transformer layers (see Figures 3 and 7). The transformers with positional encodings gave surprisingly little attention to the resp tokens when producing resp and EOS tokens. This pattern of attention is supportive of the idea that they are not encoding a cumulative state variable of the count within each time step. As predicted, swapping two non-terminal hidden states within the same phase did not appreciably change the position of the models' EOS token predictions. We can see the results of these interventions in Figure 4. We include an additional DAS analysis on the Last Value variable from the specific form of the Ctx-Distr program in the RoPE Transformers and GRUs. The resulting IIA for the Multi-Object transformers was a value of 0.827. The relatively low IIA is supportive of the notion that the Multi-Object transformers partially rely on a positional readout to solve the task. We introduce a Variable-Length variant of the Multi-Object

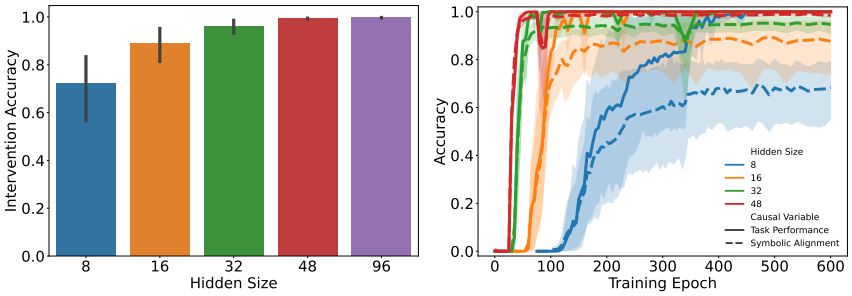

Figure 5: Left: Interchange intervention accuracy (IIA) on the Up-Down program in the GRU models on the Multi-Object task as a function of increasing hidden state dimensionality (model size). We see that the mean of the IIA increases as the number of dimensions increases while the variability decreases with increasing model size. Right: Both task accuracy and IIA (symbolic alignment) on held out data over the course of training for different model sizes (also GRUs on the Multi-Object task). We see a correlation between the first epoch with non-zero in both the IIA and task accuracy; the first non-zero epoch occurs more consistently, earlier with greater model size; and we see greater variability in the IIA with smaller model sizes.

task where non-counting tokens can appear with some probability at each step in the demo phase to break count-position correlations. These Variable-Length transformers achieved an IIA of 0.960 (see Figure 10). In addition, we provide a theoretical analysis with simulations of No Positional Encoding (NoPE) transformers in Supplement A.4. We use these results to support the claims in Figure 1.

We include an analysis involving the direct substitution of activation values in the models' representations. Of all the neurons and models we analyzed, the best IIA was 0.399 in these interventions. This IIA was achieved when transferring the activations for neurons 12 and 18 in the LSTM model shown in Figure 2. We use Figure 2 to highlight the importance of learning the rotation in DAS. Interpreting and intervening on the activations directly is a difficult task that can be misleading.

4.2 Model Dimensionality and Learning Trajectories

We can see from Figure 5 that although many model sizes can solve the Multi-Object task, increasing the number of dimensions in the hidden states of the GRUs improves IIA in alignments with the Up-Down program. We can also see in Figure 6 that the larger models tend to have less graded alignments. We examine the symbolic alignments over the course of training in Figure 5. Of note is the correlation between alignment and performance. This is especially pronounced in the larger models. And we note the relatively flat curves of the alignment trajectories after the models solve the task.

4.3 Tasks

An interesting result is the impact of demonstration token type on the resulting alignment of the recurrent models with the Up-Down program. We can see from Figure 4 that recurrent models trained on the Same-Object task—in which the demo tokens are the same type as the resp tokens—have poor alignment with any of the proposed symbolic programs. We use this result to highlight the significance of the unified, interchangeable numeric representations found in the Multi-Object and Single-Object tasks.

We present a number of theoretical neural solutions to the counting task in Figure 3 as examples of possible neural solutions to each of the tasks. The Overlap Solution, shown in blue in Panel 3(a), is an example of how some solutions may fail to align with the Up-Down solution. In the Overlap Solution, we see that the Count is entangled with the phase of the trial due to the overlap of the trajectory on the vertical axis. In this model, we would be unable to distinguish between a count of n in the demo phase and a count of $n + 1$ in the response phase at the overlapping points in the trajectories. We do not make claims in this work about how the Same-Object models are solving the task.

4.4 SYMBOLIC GRADIENCE

We now shift towards a more nuanced perspective of symbolic alignments with neural systems, where we highlight the graded nature of the neural symbols. We can see from Figure 6 that the GRU models trained on the Multi-Object task have worse IIA when the quantities involved in the intervention are larger, and when the intervention quantities have a greater absolute difference. We point out that the task training data forces the models to have more experience with smaller numbers, as they necessarily interact with smaller numbers every time they interact with larger numbers. This is perhaps a causal factor for the more graded representations at larger numbers. The DAS training data suffers from a similar issue, where we use a uniform sampling of the target quantities that define the training sequences and then we uniformly sample the intervention indices from these sequences. This results in a disproportionately large number of training interventions containing smaller values.

5 DISCUSSION/CONCLUSION

In this work we used causal methods to demonstrate the existence of symbol-like variables within NN solutions to numeric equivalence tasks. We showed that these numeric neural variables emerge purely from an NTP objective and represent abstract information that is only latent in the task structure. These findings are a proof of principle that neural systems do not need explicit exposure to discrete numeric symbols for symbol-like representations of number to emerge. Nor do neural systems need built-in counting principles to inform their numeric learning.

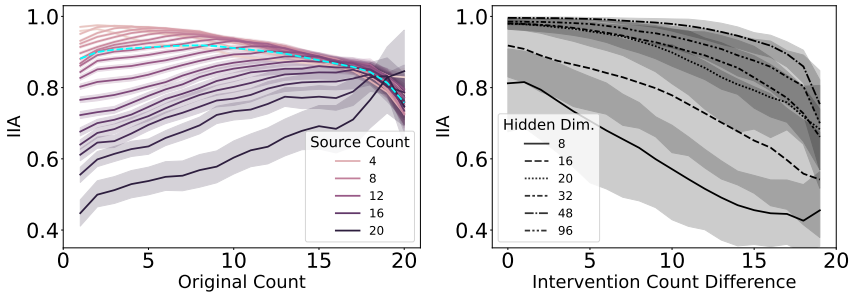

Figure 6: *Left*: DAS IIA where the x-axis shows the existing count in the original sequence before the interchange intervention. The colors denote the counts that replace the original count after the intervention. The data is from GRUs trained on the Multi-Object task of all reported sizes that are listed in in the right panel. The cyan, dashed line represents the mean IIA, highlighting the greater number of samples for the lower number interventions. *Right:* DAS IIA where the x-axis shows the absolute difference in magnitude between the original, pre-existing count and the source count (the count used to replace the original). The different dashes indicate different model sizes. We can see from both panels that the contents of the interventions affect the IIA in a relatively smooth fashion.

We also demonstrated differences in the high-level solutions used by different model architectures in different tasks. Namely, we showed that increasing the dimensionality of the recurrent models improved their symbolic alignment, we showed that transformers solved the tasks by recomputing the relevant information at each step in the sequence—contrasted against the cumulative count variables discovered in the recurrent models—and we showed that different solutions arise in the Same-Object Task compared to the other two. An interesting phenomenon in the LLM literature is the effect of model scale on performance (Brown et al., 2020; Kaplan et al., 2020). Although our scaling results are for GRUs on toy tasks, they are provocative for understanding why size might improve autoregressive results. Perhaps increased dimensionality allows the models to find more symbol-like, disentangled solutions when solving their next-token prediction tasks. This is consistent with the early learning and strong correlation between performance and symbolic alignment demonstrated in larger models in Figure 5. We conjecture the possibility that this result can be explained by the lottery ticket hypothesis (Frankle & Carbin, 2019) combined with lazy learning dynamics (Jacot et al., 2020). Perhaps the majority of what these models learn are linear functions of their initial features, and increasing the dimensionality of the model increases the number of potential pathways/features that the model can use to solve the task.

We are unsure if the "stateless", time-distributed solution exhibited by the transformers generalizes beyond the counting tasks presented in this work. It is possible that this finding is representative of a more general principle—that transformers avoid solutions that use cumulative, Markovian state variables. We provide an analysis in Supplement A.4 of a one-layer transformer without positional encodings trained on a variant of the Single-Object task without a BOS token, and without a T token. We experimentally and mathematically support the idea that this minimal model solves the task by assigning opposite numeric values to the demo and resp tokens and averaging their values at each step in the sequence. Although it seems as though the transformers presented in Figure 4 might rely in part on a positional readout from the relatively low alignment with the Last Value variable in Figure 10, we managed to get a much higher alignment when using transformers trained on a variant of the task that breaks correlations between the position and count of the sequence (see Supplement A.6). We find it worth noting that the Ctx-Distr solution exhibited by the transformers lends itself to the type of solutions that might be predicted by RASP-L (Zhou et al., 2023).

Models trained on the Same-Object Task failed to align with any of the symbolic algorithms that we presented in this paper. To address this, we included Figure 3 showing the first two principal components of a Same-Object GRU model over different trial trajectories. We also included a number of theoretical models to assist conceptualization of why some symbolic algorithms might align with the neural solutions whereas others would not. We note that there are symbolic programs that use memorization that could trivially align with each of the recurrent models. One such solution might involve a single variable that encodes each possible Count-Phase combination. In this case, the alignment would simply learn to transfer the complete state at each causal intervention. As mentioned earlier in this work, we are only concerned with solutions that are causally distinct from one another. We leave a more thorough, causal analysis of the Same-Object models to future work.

An important aspect of our work is demonstrating the potential for misleading conclusions in the absence of causal analysis methods. We can see this in Figure 2 where the activations for the LSTM might be mistaken for being sufficient to change the model's count. Similarly, the PCA projections in Figure 3 might fail to provide predictions of neural variable interchangeability, and the attention weights might mislead on token value interchangeability. We note, however, that these non-causal techniques are fruitful for exploration and conceptualization, complementing causal methods.

We now expand upon the learning trajectories displayed in Figure 5. We can see from the performance curves that both the models' task performance and alignment performance begin a transition away from 0% at similar epochs and plateau at similar epochs. This result can be contrasted with an alternative result in which the alignment curves significantly lagged behind the task performance of the models. Alternatively, there could have been a stronger upward slope of the IIA following the initial performance jump. In these hypothetical cases, a possible interpretation could have been that the network first develops more complex solutions or unique solutions for many different input-output pairs, and subsequently unifies them over training. The pattern we observe instead is consistent with the idea that the networks are biased towards the simplest, unified strategies from the beginning of training. Perhaps our result is to be expected in light of works like Saxe et al. (2019) and Saxe et al. (2022) which show an inherent tendency for NNs trained via gradient descent to find solutions that share network pathways. This would explain the driving force towards the demo and response phases sharing the same representation of a Countvariable.

Lastly, we demonstrated that the symbol-like, neural subspaces illuminated by DAS are not always perfectly symbolic, often exhibiting a smooth, graded influence from the content of the variables being intervened upon. We interpret these results as a reminder that representations in distributed systems exist on a continuum despite seemingly discrete, symbolic performance on tasks. These results have an analogy to children's number cognition in which children may appear to possess a symbol-like understanding of exact numbers and their associated principles, but when probed deeper, the symbol-like picture falls apart (Wynn, 1992; Davidson et al., 2012). Perhaps the graded nature of the neural representations reinforces the utility of thinking about network solutions as trajectories in a dynamical system, where the values along a set of dimensions are analogous to the values of high-level, causal variables. We use our findings about symbolic gradience as a reminder that although NNs may discover approximations to interpretable, symbol-like solutions, their representations are still ultimately graded—adding nuance to the effort to find in them exact implementations of any symbolic computer program.

REFERENCES

Laith Alzubaidi, Jinglan Zhang, Amjad J Humaidi, Ayad Al-Dujaili, Ye Duan, Omran Al-Shamma, J Santamaría, Mohammed A Fadhel, Muthana Al-Amidie, and Laith Farhan. Review of deep learning: concepts, CNN architectures, challenges, applications, future directions. *Journal of Big Data*, 8(1):53, 2021. ISSN 2196-1115. doi: 10.1186/s40537-021-00444-8. URL https://doi.org/10.1186/s40537-021-00444-8.

Jimmy Lei Ba, Jamie Ryan Kiros, and Geoffrey E. Hinton. Layer normalization, 2016. URL https://arxiv.org/abs/1607.06450.

Freya Behrens, Luca Biggio, and Lenka Zdeborová. Counting in small transformers: The delicate interplay between attention and feed-forward layers, 2024. URL https://arxiv.org/abs/2407.11542.

Adithya Bhaskar, Dan Friedman, and Danqi Chen. The heuristic core: Understanding subnetwork generalization in pretrained language models, 2024. URL https://arxiv.org/abs/2403.03942.

Tom B. Brown, Benjamin Mann, Nick Ryder, Melanie Subbiah, Jared Kaplan, Prafulla Dhariwal, Arvind Neelakantan, Pranav Shyam, Girish Sastry, Amanda Askell, Sandhini Agarwal, Ariel Herbert-Voss, Gretchen Krueger, Tom Henighan, Rewon Child, Aditya Ramesh, Daniel M. Ziegler, Jeffrey Wu, Clemens Winter, Christopher Hesse, Mark Chen, Eric Sigler, Mateusz Litwin, Scott Gray, Benjamin Chess, Jack Clark, Christopher Berner, Sam McCandlish, Alec Radford, Ilya Sutskever, and Dario Amodei. Language models are few-shot learners, 2020.

Kyunghyun Cho, Bart van Merrienboer, Çaglar Gülçehre, Fethi Bougares, Holger Schwenk, and Yoshua Bengio. Learning phrase representations using RNN encoder-decoder for statistical machine translation. *CoRR*, abs/1406.1078, 2014. URL http://arxiv.org/abs/1406.1078.

Kathryn Davidson, Kortney Eng, and David Barner. Does learning to count involve a semantic induction? *Cognition*, 123(1):162–173, 2012. ISSN 0010-0277. doi: https://doi.org/10.1016/j.cognition.2011.12.013.

Alessandro Di Nuovo and Tim Jay. Development of numerical cognition in children and artificial systems: a review of the current knowledge and proposals for multi-disciplinary research. *Cognitive Computation and Systems*, 1(1):2–11, 2019. doi: https://doi.org/10.1049/ccs.2018.0004. URL https://ietresearch.onlinelibrary.wiley.com/doi/abs/10.1049/ccs.2018.0004.

Alessandro Di Nuovo and James L. McClelland. Developing the knowledge of number digits in a child-like robot. *Nature Machine Intelligence*, 1(12):594–605, 2019. ISSN 2522-5839. doi: 10.1038/s42256-019-0123-3. URL http://dx.doi.org/10.1038/s42256-019-0123-3.

Quan Do and Michael E. Hasselmo. Neural Circuits and Symbolic Processing. *Neurobiology of learning and memory*, 186:107552, December 2021. ISSN 1074-7427. doi: 10.1016/j.nlm.2021.107552. URL https://www.ncbi.nlm.nih.gov/pmc/articles/PMC10121157/.

Nadine El-Naggar, Andrew Ryzhikov, Laure Daviaud, Pranava Madhyastha, and Tillman Weyde. Formal and empirical studies of counting behaviour in relu rnns. In François Coste, Faissal Ouardi, and Guillaume Rabusseau (eds.), *Proceedings of 16th edition of the International Conference on Grammatical Inference*, volume 217 of *Proceedings of Machine Learning Research*, pp. 199–222. PMLR, 10–13 Jul 2023. URL https://proceedings.mlr.press/v217/el-naggar23a.html.

Nelson Elhage, Tristan Hume, Catherine Olsson, Nicholas Schiefer, Tom Henighan, Shauna Kravec, Zac Hatfield-Dodds, Robert Lasenby, Dawn Drain, Carol Chen, Roger Grosse, Sam McCandlish, Jared Kaplan, Dario Amodei, Martin Wattenberg, and Christopher Olah. Toy models of superposition. *Transformer Circuits Thread*, 2022. https://transformer-circuits.pub/2022/toy_model/index.html.

M. Fang, Z. Zhou, S. Chen, and J. L. McClelland. Can a recurrent neural network learn to count things? *Proceedings of the 40th Annual Conference of the Cognitive Science Society*, pp. 360–365, 2018.

Jerry A. Fodor. *The Language of Thought*. Harvard University Press, 1975. ISBN 978-0-674-51030-2. Google-Books-ID: XZwGLBYLbg4C.

Jerry A. Fodor. *Psychosemantics: The Problem of Meaning in the Philosophy of Mind*. MIT Press, 1987.

Jerry A. Fodor and Zenon W. Pylyshyn. Connectionism and cognitive architecture: A critical analysis. *Cognition*, 28(1):3–71, March 1988. ISSN 0010-0277. doi: 10.1016/0010-0277(88)90031-5. URL https://www.sciencedirect.com/science/article/pii/0010027788900315.

Jonathan Frankle and Michael Carbin. The lottery ticket hypothesis: Finding sparse, trainable neural networks, 2019. URL https://arxiv.org/abs/1803.03635.

Atticus Geiger, Hanson Lu, Thomas Icard, and Christopher Potts. Causal abstractions of neural networks. *CoRR*, abs/2106.02997, 2021. URL https://arxiv.org/abs/2106.02997.

Atticus Geiger, Zhengxuan Wu, Christopher Potts, Thomas Icard, and Noah D. Goodman. Finding alignments between interpretable causal variables and distributed neural representations, 2023.

Mor Geva, Jasmijn Bastings, Katja Filippova, and Amir Globerson. Dissecting recall of factual associations in auto-regressive language models, 2023. URL https://arxiv.org/abs/2304.14767.

Peter Gordon. Numerical cognition without words: Evidence from Amazonia. *Science*, 306(5695): 496–499, 2004. ISSN 00368075. doi: 10.1126/science.1094492.

Sepp Hochreiter and Jürgen Schmidhuber. Long short-term memory. *Neural Comput.*, 9(8): 1735–1780, nov 1997. ISSN 0899-7667. doi: 10.1162/neco.1997.9.8.1735. URL https://doi.org/10.1162/neco.1997.9.8.1735.

Arthur Jacot, Franck Gabriel, and Clément Hongler. Neural tangent kernel: Convergence and generalization in neural networks, 2020. URL https://arxiv.org/abs/1806.07572.

Jared Kaplan, Sam McCandlish, Tom Henighan, Tom B. Brown, Benjamin Chess, Rewon Child, Scott Gray, Alec Radford, Jeffrey Wu, and Dario Amodei. Scaling laws for neural language models, 2020.

Neehar Kondapaneni and Pietro Perona. A Number Sense as an Emergent Property of the Manipulating Brain. *arXiv*, pp. 1–23, 2020. URL http://arxiv.org/abs/2012.04132.

Brenden M. Lake, Tomer D. Ullman, Joshua B. Tenenbaum, and Samuel J. Gershman. Building machines that learn and think like people. *Behavioral and Brain Sciences*, 40:e253, January 2017. ISSN 0140-525X, 1469-1825. doi: 10.1017/S0140525X16001837. URL https://www.cambridge.org/core/journals/behavioral-and-brain-sciences/article/building-machines-that-learn-and-think-like-people/A9535B1D745A0377E16C590E14B94993.

Gary Marcus. Deep learning: A critical appraisal, 2018. URL https://arxiv.org/abs/1801.00631.

J. L. McClelland, D. E. Rumelhart, and PDP Research Group (eds.). *Parallel Distributed Processing. Volume 2: Psychological and Biological Models*. MIT Press, Cambridge, MA, 1986.

Kevin Meng, David Bau, Alex Andonian, and Yonatan Belinkov. Locating and editing factual associations in gpt, 2023. URL https://arxiv.org/abs/2202.05262.

William Merrill, Nikolaos Tsilivis, and Aman Shukla. A tale of two circuits: Grokking as competition of sparse and dense subnetworks, 2023. URL https://arxiv.org/abs/2303.11873.

Khaled Nasr, Pooja Viswanathan, and Andreas Nieder. Number detectors spontaneously emerge in a deep neural network designed for visual object recognition. *Science Advances*, 5(5):1–11, 2019. ISSN 23752548. doi: 10.1126/sciadv.aav7903.

Allen Newell. Physical symbol systems. *Cognitive Science*, 4(2):135–183, April 1980. ISSN 0364-0213. doi: 10.1016/S0364-0213(80)80015-2. URL https://www.sciencedirect.com/science/article/pii/S0364021380800152.

Allen Newell. The knowledge level. *Artificial Intelligence*, 18(1):87–127, January 1982. ISSN 0004-3702. doi: 10.1016/0004-3702(82)90012-1. URL https://www.sciencedirect.com/science/article/pii/0004370282900121.

Chris Olah. Distributed representations: Composition superposition. https://transformer-circuits.pub/2023/superposition-composition, 2023.

Chris Olah, Alexander Mordvintsev, and Ludwig Schubert. Feature visualization. *Distill*, 2017. doi: 10.23915/distill.00007. https://distill.pub/2017/feature-visualization.

Chris Olah, Arvind Satyanarayan, Ian Johnson, Shan Carter, Ludwig Schubert, Katherine Ye, and Alexander Mordvintsev. The building blocks of interpretability. *Distill*, 2018. doi: 10.23915/distill.00010. https://distill.pub/2018/building-blocks.

Chris Olah, Nick Cammarata, Ludwig Schubert, Gabriel Goh, Michael Petrov, and Shan Carter. Zoom in: An introduction to circuits. *Distill*, 2020. doi: 10.23915/distill.00024.001. https://distill.pub/2020/circuits/zoom-in.

Adam Paszke, Sam Gross, Francisco Massa, Adam Lerer, James Bradbury, Gregory Chanan, Trevor Killeen, Zeming Lin, Natalia Gimelshein, Luca Antiga, Alban Desmaison, Andreas Köpf, Edward Z. Yang, Zach DeVito, Martin Raison, Alykhan Tejani, Sasank Chilamkurthy, Benoit Steiner, Lu Fang, Junjie Bai, and Soumith Chintala. Pytorch: An imperative style, high-performance deep learning library. *CoRR*, abs/1912.01703, 2019. URL http://arxiv.org/abs/1912.01703.

Judea Pearl. An Introduction to Causal Inference. *The International Journal of Biostatistics*, 6(2):7, February 2010. ISSN 1557-4679. doi: 10.2202/1557-4679.1203. URL https://www.ncbi.nlm.nih.gov/pmc/articles/PMC2836213/.

Zenon W. Pylyshyn. Computation and cognition: Issues in the foundations of cognitive science. *Behavioral and Brain Sciences*, 3(1):111–169, 1980. ISSN 1469-1825. doi: 10.1017/S0140525X00002053. Place: United Kingdom Publisher: Cambridge University Press.

D. E. Rumelhart, J. L. McClelland, and PDP Research Group (eds.). *Parallel Distributed Processing. Volume 1: Foundations*. MIT Press, Cambridge, MA, 1986.

Silvester Sabathiel, James L. McClelland, and Trygve Solstad. Emerging Representations for Counting in a Neural Network Agent Interacting with a Multimodal Environment. *Artificial Life Conference Proceedings*, ALIFE 2020: The 2020 Conference on Artificial Life:736–743, 07 2020. doi: 10.1162/isal_a_00333. URL https://doi.org/10.1162/isal_a_00333.

Andrew M. Saxe, James L. McClelland, and Surya Ganguli. A mathematical theory of semantic development in deep neural networks. *Proceedings of the National Academy of Sciences*, 116 (23):11537–11546, May 2019. ISSN 1091-6490. doi: 10.1073/pnas.1820226116. URL http://dx.doi.org/10.1073/pnas.1820226116.

Andrew M. Saxe, Shagun Sodhani, and Sam Lewallen. The neural race reduction: Dynamics of abstraction in gated networks. 2022.

Adam Scherlis, Kshitij Sachan, Adam S. Jermyn, Joe Benton, and Buck Shlegeris. Polysemanticity and capacity in neural networks, 2023. URL https://arxiv.org/abs/2210.01892.

Paul Smolensky. On the proper treatment of connectionism. 1988.

Jianlin Su, Yu Lu, Shengfeng Pan, Ahmed Murtadha, Bo Wen, and Yunfeng Liu. Roformer: Enhanced transformer with rotary position embedding, 2023.

Hugo Touvron, Thibaut Lavril, Gautier Izacard, Xavier Martinet, Marie-Anne Lachaux, Timothée Lacroix, Baptiste Rozière, Naman Goyal, Eric Hambro, Faisal Azhar, Aurelien Rodriguez, Armand Joulin, Edouard Grave, and Guillaume Lample. Llama: Open and efficient foundation language models, 2023.

Alexander Trott, Caiming Xiong, and Richard Socher. Interpretable counting for visual question answering. *6th International Conference on Learning Representations, ICLR 2018 - Conference Track Proceedings*, pp. 1–18, 2018.

Ashish Vaswani, Noam Shazeer, Niki Parmar, Jakob Uszkoreit, Llion Jones, Aidan N. Gomez, Lukasz Kaiser, and Illia Polosukhin. Attention is all you need. *CoRR*, abs/1706.03762, 2017. URL http://arxiv.org/abs/1706.03762.

Jesse Vig, Sebastian Gehrmann, Yonatan Belinkov, Sharon Qian, Daniel Nevo, Simas Sakenis, Jason Huang, Yaron Singer, and Stuart Shieber. Causal mediation analysis for interpreting neural nlp: The case of gender bias, 2020. URL https://arxiv.org/abs/2004.12265.

Kevin Wang, Alexandre Variengien, Arthur Conmy, Buck Shlegeris, and Jacob Steinhardt. Interpretability in the wild: a circuit for indirect object identification in gpt-2 small, 2022. URL https://arxiv.org/abs/2211.00593.

Gail Weiss, Yoav Goldberg, and Eran Yahav. On the practical computational power of finite precision rnns for language recognition, 2018. URL https://arxiv.org/abs/1805.04908.

Zhengxuan Wu, Atticus Geiger, Thomas Icard, Christopher Potts, and Noah D. Goodman. Interpretability at scale: Identifying causal mechanisms in alpaca, 2024. URL https://arxiv.org/abs/2305.08809.

Karen Wynn. Children's acquisition of the number words and the counting system. *Cognitive psychology*, 24(2):220–251, 1992.

Yan Zhang, Jonathon Hare, and Adam Prügel-Bennett. Learning to count objects in natural images for visual question answering. *6th International Conference on Learning Representations, ICLR 2018 - Conference Track Proceedings*, pp. 1–17, 2018.

Hattie Zhou, Arwen Bradley, Etai Littwin, Noam Razin, Omid Saremi, Josh Susskind, Samy Bengio, and Preetum Nakkiran. What algorithms can transformers learn? a study in length generalization. In *ICLR, NeurIPS Workshop*, 2023. URL https://arxiv.org/abs/2310.16028.

A APPENDIX / SUPPLEMENTAL MATERIAL

A.1 ADDITIONAL FIGURES

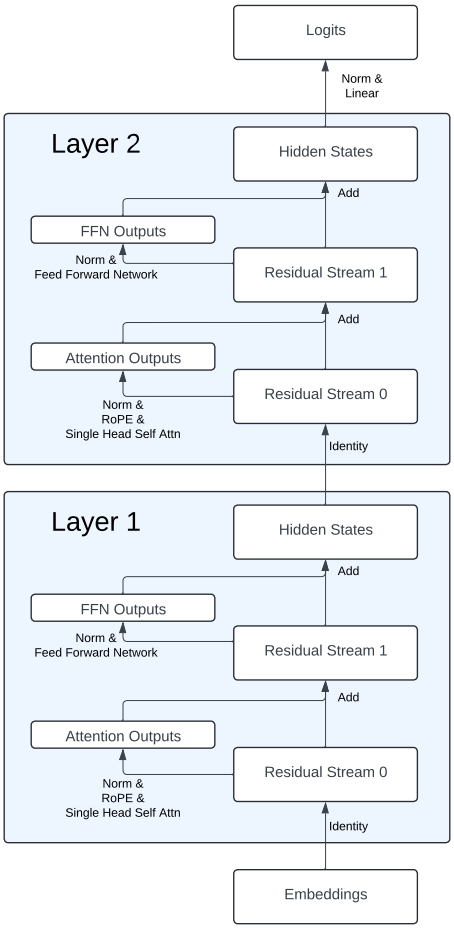

Figure 7: Diagram of the main transformer architecture used in this work. The white rectangles represent activation vectors. The arrows represent model operations. Unless otherwise stated, all interchange interventions were performed on the Hidden State activations from Layer 1 or the Residual Stream 0 within Layer 1 for the key and value projections. All normalizations are Layer Norms (Ba et al., 2016).

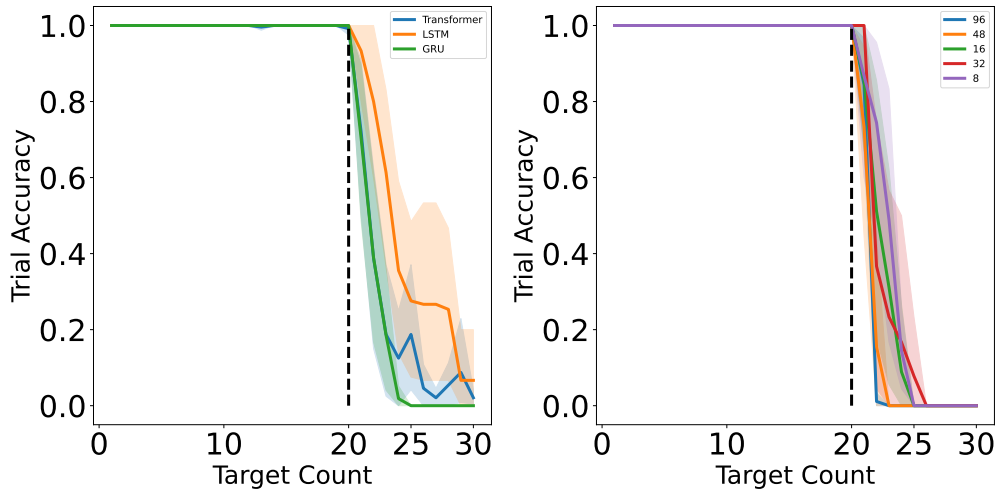

Figure 8: *Left:* The model performance on the tasks. This result includes the Multi-Object, Single-Object, and Same-Object tasks. Each target quantity includes 15 sampled sequences (even when only one configuration exists for that target quantity). 3 model seeds were dropped from the LSTM models in the Same-Object task due to lower than 99% accuracy. One seed was dropped from the transformer models in each the Single-Object and Same-Object tasks for the same reason. *Right:* The GRU performance on the tasks facetted by model size (hidden dimensionality). This result is only for GRUs train on the Multi-Object task.

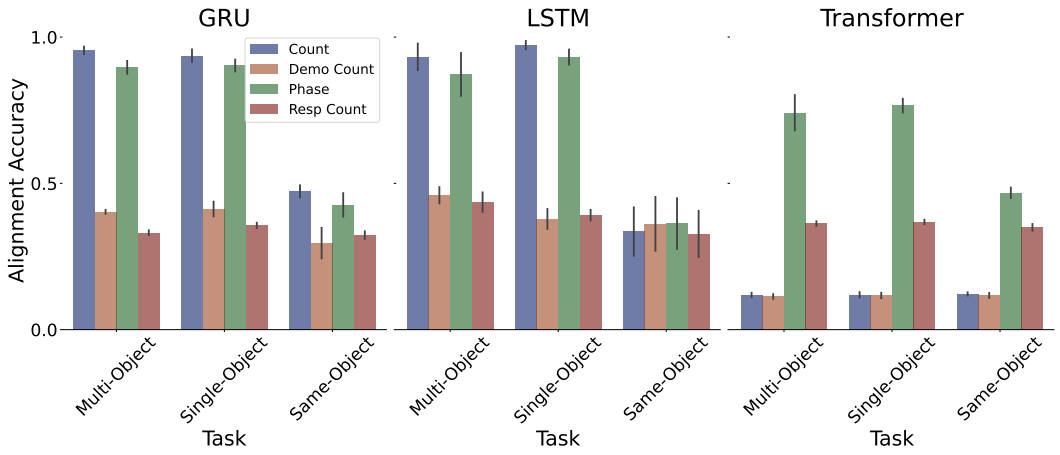

Figure 9: Interchange intervention accuracy (IIA) on variables from different symbolic programs for different tasks faceted by architecture type. The y-axis shows the proportion of trials in which the model predicts all counterfactual tokens correctly after a causal intervention for the corresponding variable on held out data.

A.2 Model Details

All artificial neural network models were implemented and trained using PyTorch (Paszke et al., 2019) on Nvidia Titan X GPUs. Unless otherwise stated, all models used an embedding and hidden state size of 20 dimensions. To make the token predictions, each model used a two layer multi-layer perceptron (MLP) with GELU nonlinearities, with a hidden layer size of 4 times the hidden state dimensionality with 50% dropout on the hidden layer. The GRU and LSTM model variants each consisted of a single recurrent cell followed by the output MLP. Unless otherwise stated, the transformer architecture consisted of two layers using Rotary positional encodings (Su et al., 2023). Each model variant used the same learning rate scheduler, which consisted of the original transformer (Vaswani et al., 2017) scheduling of warmup followed by decay. We used 100 warmup steps, a maximum learning rate of

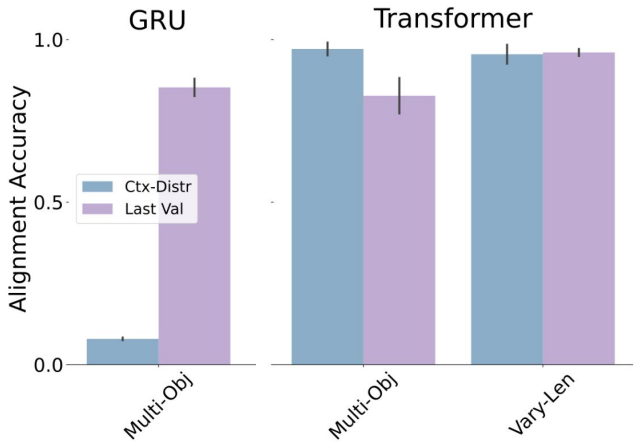

Figure 10: Interchange intervention accuracy (IIA) comparing the Ctx-Distr results from the GRU and Transformer architectures displayed in Figure 4 with the DAS alignment to the Last Value variable. We include results from a transformer trained on the Variable-Length version of the Multi-Object Task. The Ctx-Distr interventions consist of full replacements of the hidden states to determine the degree to which the models accumulate a state encoding of the important information for the task. The Last Value variable is a value of +1, -1, or 0 assigned to each incoming token. We apply DAS on the model embeddings, and only to the embeddings leading into the key and value projections in the transformers. We can see that although the Variable-Length and Multi-Object transformers both use an anti-Markovian solution (they avoid using a cumulative state) as demonstrated by the Ctx-Distr interventions, the Variable-Length transformers align much better to the Last Value variable. This is consistent with an interpretation in which the Multi-Object transformers rely, to some degree, on a positional encoding readout. This reliance is broken when the task breaks the correlation between position and count. We include the GRU results to show that the GRUs also, to some degree, assign a numeric value to each incoming embedding independent of the phase.

0.001 , a minimum of 1e-7, and a decay rate of 0.5. We used a batch size of 128, which caused each epoch to consist of 8 gradient update steps.

A.3 DAS Training Details

A.3.1 Rotation Matrix Training

To train the DAS rotation matrices, we applied PyTorch's default orthogonal parametrization to a square matrix of the same size as the model's state dimensionality. PyTorch creates the orthogonal matrix as the exponential of a skew symmetric matrix. In all experiments, we selected the number of dimensions to intervene upon as half of the dimensionality of the state. We chose this value after an initial hyperparameter search that showed the number of dimensions had little impact on performance between 5-15 dimensions. We sampled 10000 sequence pairs and for each of these pairs, we uniformly sampled corresponding indices to perform the interventions. We excluded the BOS, and EOS tokens from possible intervention sample indices. When intervening upon a state in the demo phase, we uniformly sampled 0-3 steps to continue the demo phase before changing the phase by inserting the trigger token. We used a learning rate of 0.003 and a batch size of 512.

A.3.2 Symbolic Program Algorithms

A.4 Simplified Transformer

The self-attention calculation for a single query $q_r \in R^d$ from a response token, denoted by the subscript r, is as follows:

$$\text{Attention}(q_r, K, V) = V\big(\text{softmax}(\frac{K^\top q_r}{\sqrt{d}})\big) = \sum_{i=1}^{n} \frac{e^{\frac{q_r^\top k_i}{\sqrt{d}}}}{\sum_{j=1}^{n} e^{\frac{q_r^\top k_j}{\sqrt{d}}}} v_i = \sum_{i=1}^{n} \frac{s_i^r}{\sum_{j=1}^{n} s_j^r} v_i \qquad (5)$$

Algorithm 1 One sequence step of the Up-Down Program

$q \leftarrow$ Count
$p \leftarrow$ Phase
$y \leftarrow$ input token
if $y ==$ BOS **then** ▷ BOS is beginning of sequence token
  $q \leftarrow 0, p \leftarrow 0$
  return sample(D) ▷ sample a demo token
else if $y \in$ D **then** ▷ D is set of demo tokens
  $q \leftarrow q + 1$
  return sample(D)
else if $y ==$ T **then** ▷ T is trigger token
  $p \leftarrow 1$
else if $y ==$ R **then** ▷ R is response token
  $q \leftarrow q - 1$
end if
if $(q == 0)$ & $(p == 1)$ **then**
  return EOS ▷ EOS is end of sequence token
end if
return R

Algorithm 2 One sequence step of the Up-Up Program

$d \leftarrow$ Demo Count
$r \leftarrow$ Resp Count
$p \leftarrow$ Phase
$y \leftarrow$ input token
if $y ==$ BOS **then** ▷ BOS is beginning of sequence token
  $d \leftarrow 0, r \leftarrow 0, p \leftarrow 0$
  return sample(D) ▷ sample a demo token
else if $y \in$ D **then** ▷ D is set of demo tokens
  $d \leftarrow d + 1$
  return sample(D)
else if $y ==$ T **then** ▷ T is trigger token
  $p \leftarrow 1$
else if $y ==$ R **then** ▷ R is response token
  $r \leftarrow r + 1$
end if
if $(d == r)$ & $(p == 1)$ **then**
  return EOS ▷ EOS is end of sequence token
end if
return R

Algorithm 3 One sequence step of the specific Ctx-Distr Program

$v \leftarrow$ list of previous values excluding the most recent step
$\ell \leftarrow$ Last Value ▷ The value of the most recent token
$p \leftarrow$ Phase ▷ 0 indicates the demo phase, 1 is the response phase
$y \leftarrow$ input token

v.append(ℓ)
$s \leftarrow$ SUM(v)
if $y ==$ BOS **then** ▷ BOS is beginning of sequence token
    $\ell \leftarrow 0, p \leftarrow 0$
    return sample(D) ▷ sample a demo token
else if $s \leq 0$ and $p == 1$ **then** ▷ Sum is 0 or less in the response phase
    return EOS ▷ EOS is end of sequence token
else if $y ==$ T or $y ==$ R **then** ▷ T is trigger token, R is response token
    $p \leftarrow 1$
    $\ell \leftarrow -1$
    return R
else if $y \in$ D **then** ▷ D is set of demo tokens
    $\ell \leftarrow 1$
end if

if $p == 1$ **then**
    return R
else
    return sample(D)
end if

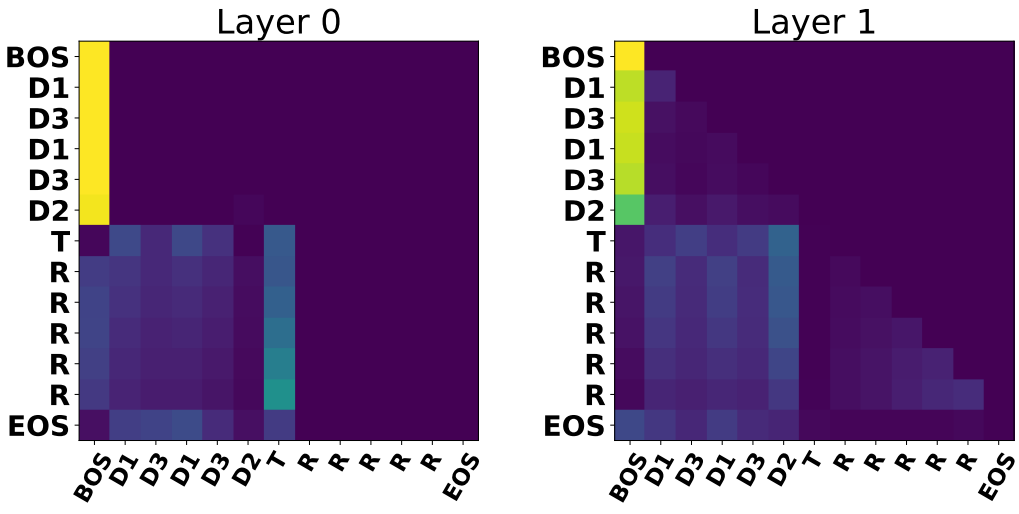

Figure 11: Attention weights for a single transformer model with two layers and using rotary positional encodings. Queries are displayed on the vertical axis in order of their appearance starting at the top. Keys are displayed on the horizontal axis starting from the left. Queries are only able to attend to themselves and preceding keys.

Where d is the dimensionality of the model, n is the sequence length, $K \in R^{d \times n}$ is a matrix of column vector keys, $V \in R^{d \times n}$ is a matrix of column vector values, and $s_i^r = e^{\frac{q_r^\top k_i}{\sqrt{d}}}$, using r to denote the token type that produced q. We refer to $s_i^r v_i$ as the strength value of the i^{th} token for the query q_r.

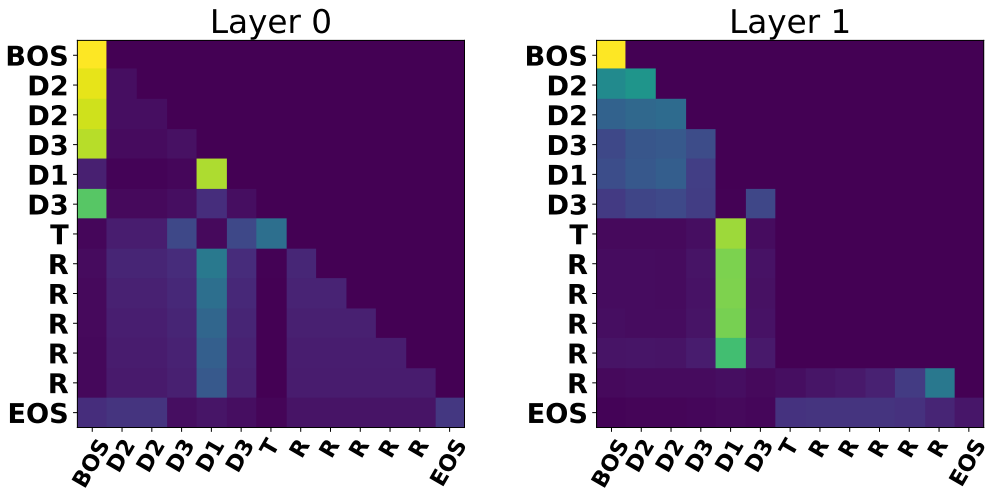

Figure 12: Attention weights for a single transformer model seed with two layers and no positional encodings (NPE). Queries are displayed on the vertical axis in order of their appearance starting at the top. Keys are displayed on the horizontal axis starting from the left. Queries are only able to attend to themselves and preceding keys.

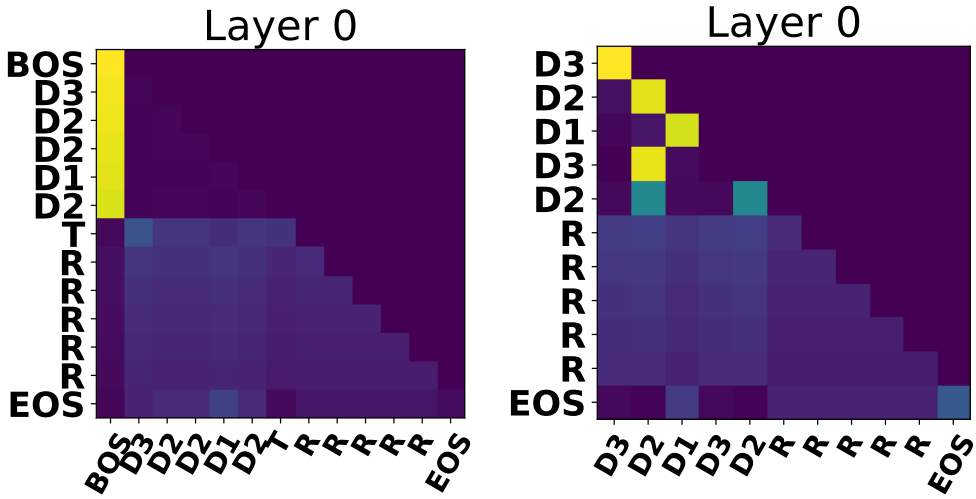

Figure 13: Left: Attention weights for a single transformer model seed with one layer and no positional encodings. Right: Attention weights for a single transformer seed with one layer and no positional encodings trained without the BOS and trigger token types. In both figures, queries are displayed on the vertical axis in order of their appearance in the sequence starting at the top. Keys are displayed on the horizontal axis starting from the left. Queries are only able to attend to themselves and preceding keys.

In a transformer without positional encodings, each of the queries for the response tokens will produce equal strength values to one another for a given key-value pair. Thus, under the assumption that the attention mechanism is performing a sum of the count contributions from each token in the sequence, we should be able to use the $s_i^r v_i$ to increment and decrement the number of tokens the model will produce for a given sequence in the following way:

$$\text{IncrementedAttention}(q_r, K, V) = \frac{1}{s_r^r + \sum_{j=1}^{n} s_j^r} \left(s_r^r v_r + \sum_{i=1}^{n} s_i v_i \right) \tag{6}$$

Where the subscript r denotes the strength s_r and value v_r were calculated from a response key-value pair. Similarly, we can decrement the count using a key-value pair from a demonstration token, D, in the following way.

$$\text{DecrementedAttention}(q_r, K, V) = \frac{1}{s_D^r + \sum_{j=1}^{n} s_j^r}\left(s_D^r v_D + \sum_{i=1}^{n} s_i v_i\right) \tag{7}$$

As a sanity check we use single layer transformers without positional encodings and add and subtract from the transformer's count using the strength values as described in this section. We are able to change the position at which it produces the EOS token with 100% accuracy.

A.5 Additional Interventions Continued

We detail in this section why our activation transfers are sufficient to demonstrate that the transformers use a solution that re-references/recomputes the relevant information to solve the tasks at each step in the sequence. The hidden states in Layer 1 are a bottleneck at which a cumulative counting variable must exist if it were to use a strategy like the Up-Down or Up-Up programs. This is because the Attention Outputs of Layer 1 are the first activations that have had an opportunity to cross communicate between token positions. This means that the representations between the Residual Stream 1 of Layer 1 up to the Residual Stream 0 of Layer 2 cannot have read off a cumulative state from the previous token position other than reading off the positional information from the previous positional encodings. The 2-layer architecture is then limited in that it has only one more opportunity to transfer information between positions—the attention mechanism in Layer 2. Thus, if a hidden state at time t were to have encoded a cumulative representation of the count that will be used by the model at time $t + 1$, that cumulative representation must exist in the activation vectors between the Residual Stream 1 in Layer 1 and the Residual Stream 0 of Layer 2. If it is using such a cumulative representation, then when we perform a full activation swap in the Layer 1 hidden states then the resulting predictions should be influenced by the swap. As Figures 4 and 14 indicate, the resulting transformer predictions are mostly unchanged by the intervention, demonstrating a recomputing of information at each step in the task.

A.6 Variable-Length Task Variants

Here we include additional tasks to prevent the transformers with positional encodings from learning a solution that relies on reading out positional information. We introduce Variable-Length variants of each of the Multi-Object, Single-Object, and Same-Object tasks. In the Variable-Length versions, each token in the demo phase has a 0.2 probability of being sampled as a unique "void" token type, V, that should be ignored when determining the target count of the sequence. The number of demo tokens will still be equal to the target count when the trigger token is presented. We include these void tokens as a way to vary the length of the demo phase for a given target count, thus breaking correlations between positional information and target quantities. As an example, consider the possible sequence with a target count of 2: "BOS V D V V D T R R EOS".

We show the transformer performance and the IIA for the Ctx-Distr interventions in Figure 14. Although we do not make strong claims about the manner in which these transformers solve these new tasks, we do highlight the fact that the transformers can no longer use a direct positional encoding readout to achieve 100% accuracy. These results are consistent with the hypothesis that the transformers are using the more specific, summing version of the Ctx-Distr strategy to solve these tasks, much as the no-positional encoding transformers do.

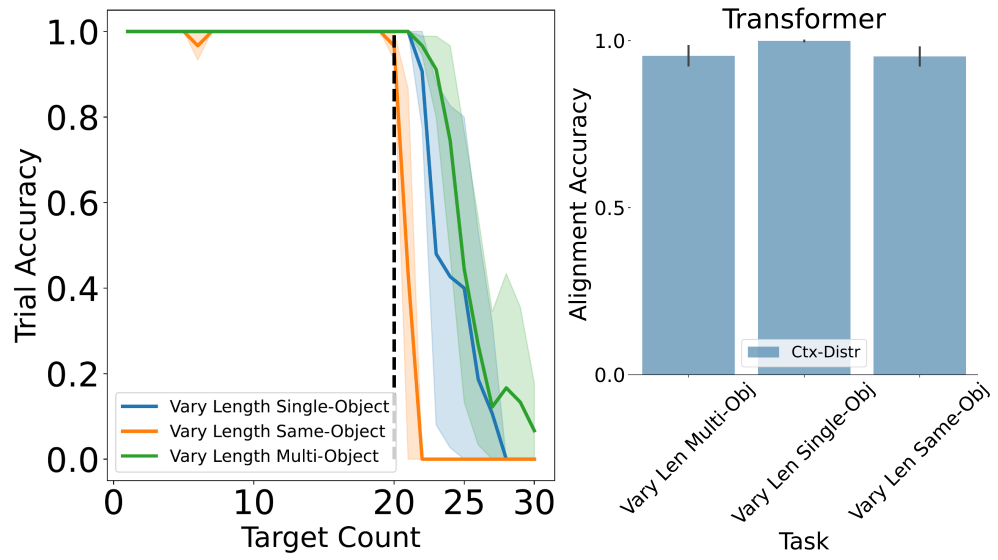

Figure 14: *Left:* The transformer performance on variable length variants of the 3 tasks. *Right:* The interchange intervention accuracy using the Ctx-Distr program for the transformer models on the variable length tasks. In both panels, 4 model seeds were dropped from the models in the variable length Same-Object task due to lower than 99% accuracy, and one seed was dropped from the variable length Single-Object task for the same reason.

A.7 Principle Components Analysis

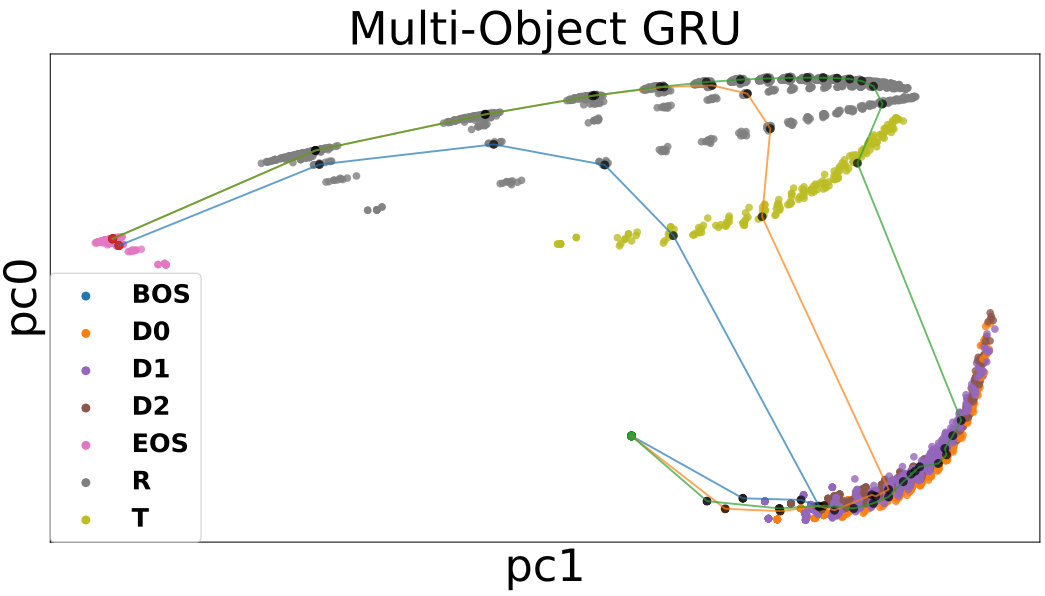

Figure 15: Principal Components Analysis of a single GRU model seed including hidden state representations over 10 trials for each target quantity from 1 to 20 in the Multi-Object task variant. Green points indicate the start of a plotted trajectory, black points indicate an intermediate step, and red points indicate the end of a plotted trajectory. The blue line plots a single trajectory from start to finish with a target quantity of 3. Similarly, the orange and green lines follow single trajectories of 7 and 15 respectively.

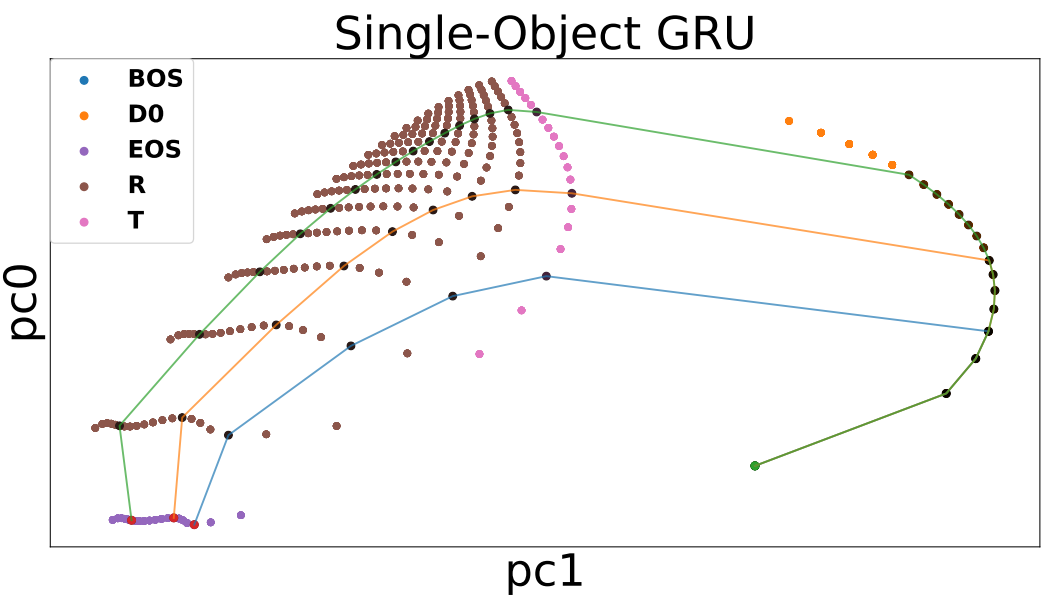

Figure 16: Principal Components Analysis of a single GRU model seed including hidden state representations over 10 trials for each target quantity from 1 to 20 in the Single Object task variant. Green points indicate the start of a plotted trajectory, black points indicate an intermediate step, and red points indicate the end of a plotted trajectory. The blue line plots a single trajectory from start to finish with a target quantity of 3. Similarly, the orange and green lines follow single trajectories of 7 and 15 respectively.

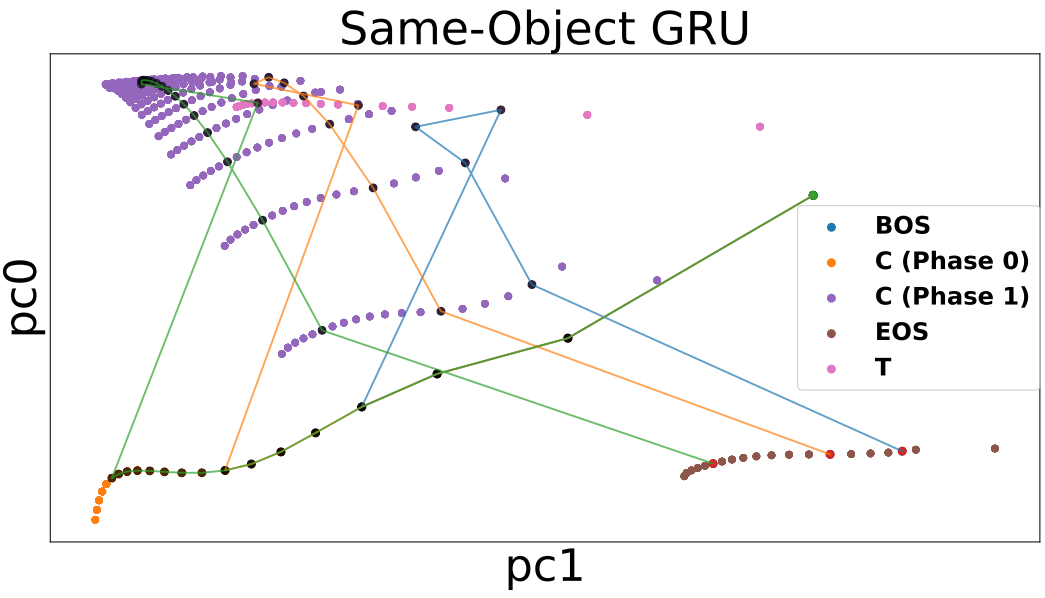

Figure 17: Principal Components Analysis of a single GRU model seed including hidden state representations over 10 trials for each target quantity from 1 to 20 in the Same-Object task variant. Green points indicate the start of a plotted trajectory, black points indicate an intermediate step, and red points indicate the end of a plotted trajectory. The blue line plots a single trajectory from start to finish with a target quantity of 3. Similarly, the orange and green lines follow single trajectories of 7 and 15 respectively.